BICEP

A Bio-Inspired Compliant Elbow Prosthesis

Castañeda, Theophil Spiegeler; Horstman, Bart; Capsi-Morales, Patricia; Santina, Cosimo Della; Piazza, Cristina

DOI
10.1007/978-3-031-55000-3_3

Publication date
2024

Document Version
Final published version

Published in
Human-Friendly Robotics 2023 - HFR

Citation (APA)
Castañeda, T. S., Horstman, B., Capsi-Morales, P., Santina, C. D., & Piazza, C. (2024). BICEP: A Bio-Inspired Compliant Elbow Prosthesis. In C. Piazza, P. Capsi-Morales, L. Figueredo, M. Keppler, & H. Schütze (Eds.), *Human-Friendly Robotics 2023 - HFR: 16th International Workshop on Human-Friendly Robotics* (pp. 36-49). (Springer Proceedings in Advanced Robotics; Vol. 29 SPAR). Springer. https://doi.org/10.1007/978-3-031-55000-3_3

BICEP: A Bio-Inspired Compliant Elbow Prosthesis

Theophil Spiegeler Castañeda[1(✉)], Bart Horstman[2], Patricia Capsi-Morales[1], Cosimo Della Santina[2,3], and Cristina Piazza[1]

[1] Department of Computer Engineering, School of Computation Information and Technology and Munich Institute of Robotics and Machine Intelligence, Technical University of Munich (TUM), Munich, Germany
theophil.spiegeler-castaneda@tum.de

[2] Department of Cognitive Robotics, Delft University of Technology (TU Delft), Delft, The Netherlands

[3] Institute of Robotics and Mechatronics, German Aerospace Center (DLR), Oberpfaffenhofen, Germany

Abstract. Adopting compliant structures holds the potential to enhance the robustness and interaction capabilities of the next generation of bionic limbs. Although researchers have proficiently explored this approach in the design of artificial hands, they devoted little attention to the development of more proximal joints. This work presents a compliant prosthetic elbow prototype called BICEP. The design incorporates compliant cross-axis flexural pivots that connect the upper and lower arm without direct contact between the two links. The actuation architecture, inspired by biological mechanisms, employs one actuator and two tendons to create an agonist-antagonist mechanism. This joint enables rotation along its flexion-extension axis while maintaining flexibility in out-of-plane directions, in a system with an overall weight of 351 g. A preliminary evaluation showcases lifting capacities supporting up to 2500 g, and a maximum speed of 157° per second across a 135° range of motion. The soft cross-axis flexural pivots exhibit compliant behavior in both the sagittal and transversal planes, enabling a pleasant interaction with the environment and ensuring safe absorption of unintentional impacts.

Keywords: Upper Limb Prosthetics · Bioinspired Systems · Compliant Mechanism · Soft Robotics

1 Introduction

Compensating for the loss of upper extremities is still a technological and clinical challenge [1], especially for subjects with high-level amputation, e.g. transhumeral. Although the complexity in structure and degrees of freedom (DoF) of the elbow is lower than the hand or wrist, the loss of its mobility strongly limits the fluid execution of prehensile, proprioceptive, and communication tasks [2]. As a result, subjects with limb loss need to compensate with the rest of the body parts, which leads to the development of unnatural motor control strategies and, often, to the rejection of the prostheses [3].

C. Piazza et al. (Eds.): HFR 2023, SPAR 29, pp. 36–49, 2024.
https://doi.org/10.1007/978-3-031-55000-3_3

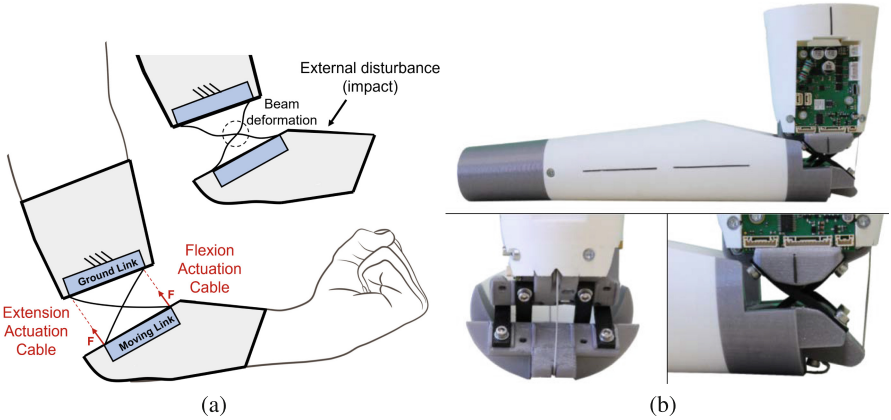

Fig. 1. (a) Schematic of cross-axis flexural pivot configuration. Deflection under normal flexion, and beam deformation under impact through external disturbances are presented. (b) Prototype of the proposed bio-inspired compliant prosthetic elbow, named BICEP. The system employs cross-axis flexural pivots for the joint design and two tendons that act as an agonist-antagonist actuation mechanism.

Despite the recent remarkable technological advancements in prosthesis design, only a few commercial solutions are available for proximal joints [4]. Commercially available elbow prostheses consist of a single rigid DoF rotational joint [5–8]. These commercial systems can cover the physiologic range of motion (RoM), but their rigid and simplified design ends up strongly decreasing usability and robustness. In addition, these systems often adopt conventional rigid sockets to interface with the user, which often limits shoulder movements in the residual limb, e.g. external rotation. A promising interfacing alternative is osseointegration, which avoids pressure on soft tissue, without limiting shoulder movements [9]. However, osseointegration transmits forces directly to skeletal segments, without damping for impact loads, which might lead to pain and discomfort [1].

To overcome the limitations of classic devices, researchers have proposed various non-conventional prosthetic elbow designs. For example, [10] exploits belt and cable-driven transmissions to achieve high output torques and speeds, while [11] uses a linkage-based transmission to optimize the efficiency. Nevertheless, because of their rigid characteristics, these solutions are still limited in everyday tasks involving interactions with the environment, other people, or the user's own body. Biomechanics show that compliance is a fundamental component of human muscle-skeletal systems, and research in hand prostheses [12–15] and wrists [16,17] have shown that mechanically replicating such compliance can drastically improve the performance. With compliance we thereby refer to the structural ability of deforming on the influence of external forces, while maintaining material integrity and joint functionality [18]. Soft robotic systems [18] are naturally more robust to collisions and allow for more natural interactions. Yet, only a few works have explored this route in the context of elbow joints. The RIC arm [19] comprises a motor-spindle combination and rigid links, but includes a limited

amount of compliance through a complaint bushing. A series elastic actuator is used in [20] and a variable stiffness mechanism is proposed in [21], both actuating a standard revolute joint. Thus, in all these devices, compliance is very localized at the motor level.

In this work, we propose an active elbow prosthesis named BICEP (Fig. 1(b)), consisting of a compact and lightweight joint with soft properties. As the human elbow joint, BICEP moves preferentially as a 1 DoF system when actuated. At the same time, the joint remains compliant in out-of-plane directions, allowing for passive excursion and compensating for the lack of shoulder external rotation that some transhumeral prosthesis socket present. This is possible through a mechanism (Fig. 1(a)) that comprises two rigid links interconnected by a compliant joint with four flexible beams arranged to form two cross-axis flexural pivots that mimic the ligaments and tendons embedded in the human elbow. BICEP results as a completely self-contained system with a flexible joint (as defined in [12]), that was characterized by different load conditions. Its range of motion, weight, and torques are compatible with physiological requirements [22].

2 Proposed Design

2.1 Model

The proposed solution can be modeled as illustrated in Fig. 2(a). Under the assumption of non-extensible tendon (blue line in panel (a)), the relative orientation q of the lower linkage w.r.t. the upper one is defined by the configuration of the motor θ via a function $h : \mathbb{R} \to \mathbb{R}$ such that $q = h(\theta)$. Note that the upper tendon is tensioned in this case. Similar calculations hold true in the other case. Moreover, we assume no CoR (Center of Rotation, O in figure) shift and a constant distance to the tendon contact points.

We proceed by writing the balance of torques around the CoR, which details the relationship of the torque of the elbow τ and the motor torque τ_{M}

$$\tau_{\mathrm{M}} = J(\theta)\tau + k(q), \tag{1}$$

where $k : \mathbb{R} \to \mathbb{R}$ is the force generated by an equivalent torsional spring representing the effect of the deformable beams in Fig. 1(a). The interested reader can find more details in [23]. The remaining term in (1) comes from $J(\theta) = \frac{\partial h}{\partial \theta} \in \mathbb{R}$, being the Jacobian of the system with $\dot{q} = J(\theta)\dot{\theta}$. Then, $J^{\intercal}(\theta)\tau$ comes from the kinetostatic duality. We removed the transpose in (1) since J is a scalar. We, therefore, need to specify h and evaluate from it J in order to have all (1) well defined.

We neglect the radius of the pulley, as illustrated in Fig. 2(b). We decide to place the two pulleys at the same distance $l_{\mathrm{op}} \in \mathbb{R}$ from the CoR. Under these assumptions, simple geometrical considerations allow us to express the length of the tendon $l \in \mathbb{R}^{+}$ as a function of the angle $q \in \mathbb{R}$ that the arm does with respect to the motor link

$$l(q) = 2l_{\mathrm{op}} \sin\left(\frac{q - \alpha - \beta}{2}\right), \tag{2}$$

where $\alpha, \beta \in \mathbb{R}$ are the two constant angles detailed in Fig. 2(b).

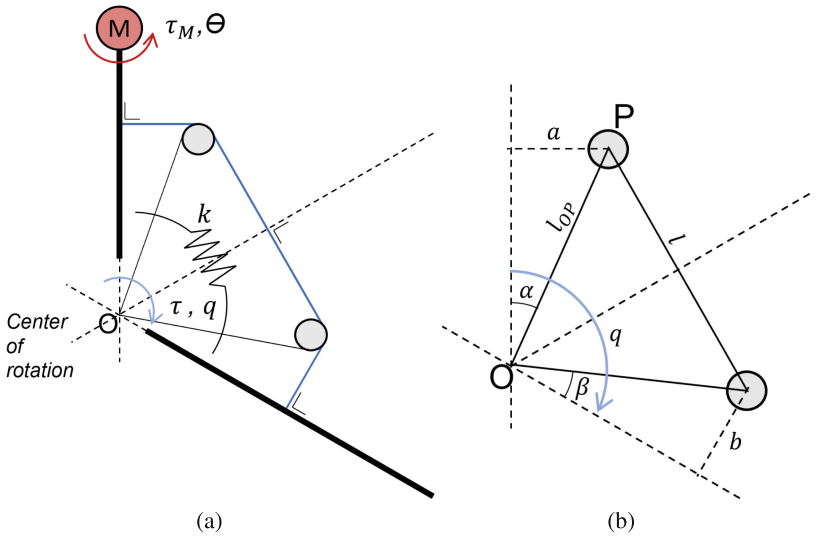

Fig. 2. Simplified model of the elbow. Panel (a) shows the motor torque τ_{M}, the output orientation θ, the stiffness parameter k, and the position of the elbow q. Panel (b) shows the length l_{op} from point P to the center of rotation and its orientation α together with the angle from the elbow to the second pulley β.

Alternatively, l can be connected to the motor rotation output θ as in

$$l(\theta) = -R_{\mathrm{M}}\theta + l_0, \tag{3}$$

where R_{M} is the radius of the motor shaft and l_0 is the length when the motor is in its homing position. By combining (2) and (3), we can derive

$$q = \underbrace{\alpha + \beta + 2\arcsin\left(\frac{-R_{\mathrm{M}}\theta + l_0}{2l_{\mathrm{op}}}\right)}_{:=h(\theta)}. \tag{4}$$

This kinematic model permits the computation of the transmission ratio between the motor speed $\dot{\theta}$ and the output speed of the elbow $\dot{q}$. The derivative results in

$$J(\theta) = 2\frac{\partial \arcsin\left(\frac{-R_{\mathrm{M}}\theta + l_0}{2l_{\mathrm{op}}}\right)}{\partial \theta} = \frac{-R_{\mathrm{M}}}{l_{\mathrm{op}}\sqrt{1 - \frac{(l_0 - R_{\mathrm{M}}\theta)^2}{4l_{\mathrm{op}}^2}}}. \tag{5}$$

Thus, plugging (5) into (1) yields the complete model of the steady state behavior of our mechanism.

We can now leverage this model to define the requirements of our device. More specifically, we find a material with which we can achieve a desired moment deflection $k(q = 135^\circ)$ of 0.854 Nm. Therefore, we calculate the Youngs Modulus (also called the

elasticity coefficient) from the four-bar model for cross-axis flexural pivots discussed in [23]. The computed Youngs Modulus lies in the range of 40 MPa, which can be achieved with TPU 58D (Extrudr FD3D GmbH, Germany). The average maximum sideway displacement (in the sagittal plane) of the human elbow is 11.2° with respect to the neutral position [24]. Therefore, the requirement for the minimum side-way RoM was set to 10°.

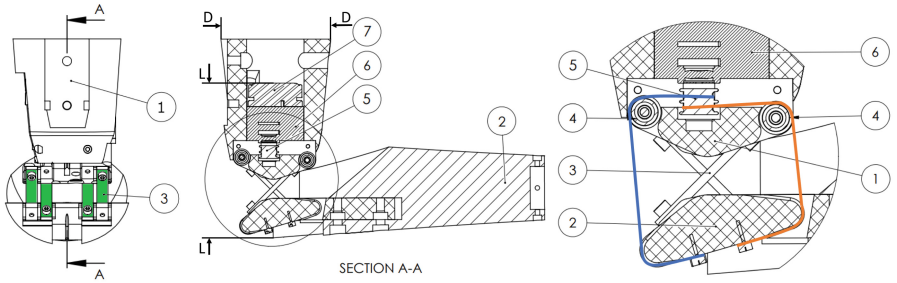

(a) (b) (c)

Fig. 3. Mechanical design of the compliant elbow joint. A back view is shown in panel (a) with the cross-axis flexural pivots (3) highlighted in green. A side view of the complete system is shown in panel (b), *L* and *D* indicate the length and diameter, respectively. Panel (c) shows a close-up of a section of the joint, where the blue and orange lines highlight the tendons used for the elbow flexion and extension. The main components are indicated: upper arm link (1) and lower arm link (2); bearing and pulley (4) for the tendon routing; motor pulley (5); Maxon GS 45 A gearbox (6) and Maxon EC 45 flat brushless DC motor (7); electronic control board from Nanotec (8). (Color figure online)

2.2 Design and Realization

Figure 3 presents a lateral and back view of the proposed system in a $q = 90°$ joint flexion configuration. The prosthetic elbow has a length of 99 mm and a diameter of 72 mm. There are two main rigid parts: the upper arm link **(1)** and the lower arm link **(2)**. They are designed with a similar profile and made from 3D-printed Polylactic Acid (PLA). These two parts are not in direct contact with each other but are interconnected by two cross-axis flexural pivots **(3)** that cross the central part of the joint. Each rectangular beam is attached to the rigid links. The flexible rectangular beams are made from 3D-printed Thermoplastic Polyurethane (TPU), a rubber-like material, selected for its elasticity and ease of manufacturing. Multiple dimensions have been experimentally tested to limit buckling under high loads, resulting in the dimensions of height $\times$ width $\times$ thickness: 45×8 x 3 mm. Like the medial collateral, lateral collateral, and annular ligaments of the physiological elbow, the two cross-axis flexural pivots offer support, stability, and flexibility to the artificial elbow joint.

The dimensions of the cross-axis flexural pivots are designed to reproduce the physiological RoM (130°–155°) of the elbow joint and cover the requirements for activities of daily living [25]. Additionally, the compliant mechanism should support high loads.

The orientation of the cross-axis flexural pivots are chosen to be 90° in the rest configuration, to give the most support when the elbow is flexed, for which, in presence of a load, the generated moment arm reaches its maximum. From the rest position, the joint can be flexed of about 45° and extended of 90°.

2.3 Actuation Architecture

Figure 3(c) shows a close-up view of the actuation components. The actuation architecture is inspired by the biological elbow joint structure and consists of two Dyneema wires, selected for their resilience. One replicates the bicep tendon (highlighted in orange) and is used for flexion movements, while the extension movements are actuated by a tendon (highlighted in blue), which replicates the tricep tendon. The two tendons system act as an agonist-antagonist mechanism, controlled by a motor **(7)**, which is widely used in robotic joint actuations [26,27]. To reduce friction and guide the routing of the tendons, two bearings **(4)** are integrated into the upper arm. Each bearing is framed in a pulley with a radius of 9 mm. To prevent misalignment and entanglement, the pulleys are displaced vertically by 2 mm with respect to each other and have a rounded profile to house the wire. According to [28], the necessary torque to perform everyday activities is 5.8 Nm which corresponds to the ability to lift up to 2000 g. The minimum speed required is 113°/s. Based on these parameters, the selected actuator **(7)** is a Maxon EC 45 flat brushless DC motor (Ø42.9 mm, 12 V, 30 W, with Hall sensors, Part number 200142) with a gearbox **(6)** Maxon GS 45 A (Ø45 mm, 0.5–2.0 Nm, Part number 678436, 32:1). A customized pulley **(5)** is attached to the motor shaft and is designed to host the two tendons. The electronic control board **(8)** from Nanotec (CL3-E-2-0F), is embedded in the lateral side of the upper arm and protected by a cover, that acts as a structural component. Finally, the terminal part of the lower arm **(2)** offers the possibility to interface a commercial wrist and/or artificial hand.

3 Experimental Validation

3.1 Prototype Specifics

BICEP features a compact and bio-inspired joint design with soft properties. The cross-axis flexural joint allows for a lightweight system, with a total weight of 351 g, in a system that can move from 0° to 135°, covering the estimated range of motion of the elbow for daily living activities [29]. This design is easy to scale and can be adapted to different sizes and requirements. Table 1 shows the final specifications of the proposed system. The specifics are compared to three systems from the current state of the art of commercial (Dynamic Arm, Ottobock [5]) and research devices (RIC arm [19], Powered Elbow[10]) for a wider perspective. A preliminary validation of the prototype was experimentally performed through a static and dynamic load test. Additionally, we evaluated the sideway displacement. A video demonstrating the functionality of BICEP is available under this link.

Table 1. Specifics of Bicep in comparison with two state-of-art systems. (L = length; D = diameter Fig. 3).

	BICEP	RIC Arm [19]	Powered Elbow [10]	Dynamic Arm (Ottobock) [5]
Weight [g]	351	746	1200	1000
Size L × D [mm]	99×72	100×76	n.a	100×80
Speed [°/s]	157	80	360	113
Lifting torque [Nm]	6.7	12	18.4	15.3
Range of motion [°]	0–135	0–135◇	15–145	15–145

◇ data extracted from video source [19], n.a. = not available

Fig. 4. Results of the static load test. The system is loaded in increments of 500 g, from 500 g to 2500 g. Mean values and the quadratic interpolation are presented with their standard deviation.

3.2 Experimental Setup

The BICEP prototype was attached to an aluminum profile and fixed to a table. The system is powered with 12 V and 4.5 A power supply. The Nanotec control board offers an API (Application Programming Interface) that allows to select from different PID (Proportional Integral Differential) control methods as position- or velocity- motor control. Furthermore, settings as the position tolerance, maximum acceleration and velocity can be configured. For the following tests, the position motor control was selected.

Because of the compliant design and the cross-axis flexural pivot not being a pure pivot joint, there is an error between the target position set by the position controller and the actual position of the forearm. To measure the absolute position of both elbow links, we used a camera setup with markers. The video recordings are analyzed using the software Tracker [30] to extract all relevant information.

BICEP was tested in combination with an adapter, mounted at the end of the lower arm, that simulates the average weight of a prosthetic hand (500 g). The adapter was also designed to allow the attachment of additional weight plates, which simulate the weight

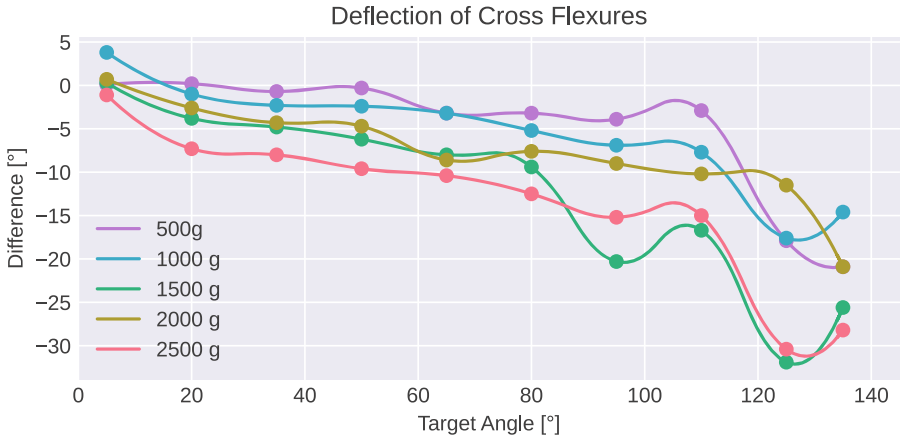

Fig. 5. Deflection of the cross flexure joint with different loads and positions. The system experiences a passive offset δ that was substracted from the deflection. δ is 7.9°, 5.5°, 4.8°, 4.0°, 2.5° for 500 g, 1000 g, 1500 g, 2000 g, 2500 g, respectively.

over a range of objects commonly used during activities of daily living. The loads were applied on the same axis, allowing a simple superposition of the torque created by the loads.

3.3 Static Load Test

To preliminary evaluate the behavior of the proposed design under different loads at selected target positions, a static load test was performed. The system was moved and held for 7 s in discrete positions with a load attached, while the required current was measured. The target positions range from an angle of 5° to 135° and are increased in steps of 15°. The system was loaded in increments of 500 g, from 500 to 2500 g. The results are presented in Fig. 4. Note that for each load condition, we measured the passive offset δ that is introduced through the spring behavior of the joint. As shown in Fig. 4, the power consumption increases with higher loads as well as its variability. Nevertheless, the current drawn by the motor does not increase proportionally with higher loads at the same target angle, as the characteristic curve of a brushless DC motor would indicate. This can be explained through the observation that the cross-axis flexures' buckling increases with higher loads, for which the joint behaves as a rolling joint. By this effect, the force transmission for different loads at the same angle becomes non-linear. For instance we observe a current drop at a target angle above 110° in the 2500 g load case. Additionally, the cross-axis joint introduces a shift of rotation axis [23], which changes the kinematics and thereby the transmitted torque. Figure 5 shows that the difference between the target and measured angle increases with higher loads and target angles. As in the current consumption, a non-linear behavior is visible with increasing loads and sinusoidal oscillations are observed for target angles above 90°. This might be related to the above described effects of the soft joint features. The maximum holding torque is 2500 g, equivalent to 9.4 Nm torque at the end-effector

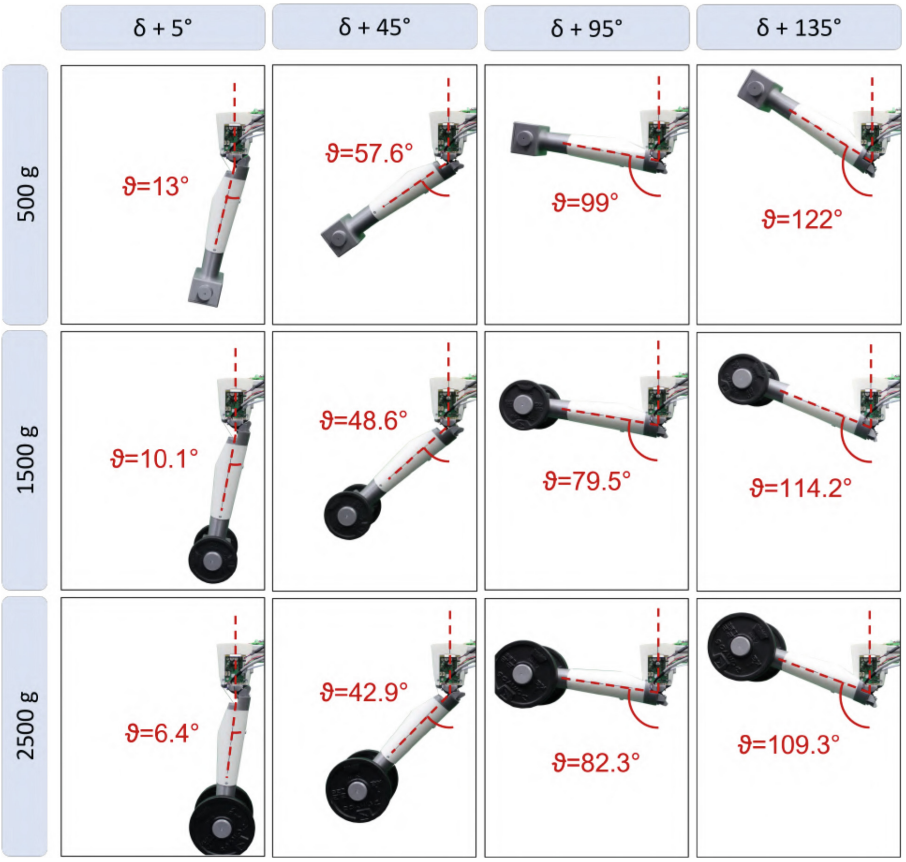

Fig. 6. Example of the cross-axis flexural pivot joint deflection for different loads and positions. Horizontal panels show BICEP with different load conditions: with only the adapter (500 g), 1500 g and 2500 g. The passive offset δ is: 7.9°, 4.8°, 2.5° for 500 g, 1500 g, 2500 g, respectively.

level, on which the motor draws 4.23 A. The measured angle for certain conditions is shown in Fig. 6.

3.4 Dynamic Load Test

The dynamic characteristics of BICEP are defined by its maximum speed, lifting capabilities, and step response. The speed was measured by moving the elbow with the motors maximum acceleration to maximum speed. The recorded speed is converted to the output speed (speed of the forearm link). A complete overview of the results in different load conditions is presented in Table 2. The maximum speed is 157°/s and corresponds to the case with a 500 g load. The speed with the maximum lifting capacity of 2500 g was measured to be 147°/s, 93% of the maximum speed.

Table 2. Results of the dynamic test with three different loads

Load [g]	500	1500	2500
Speed [°/s]	157	149	147
Rise time [s]	1.38	1.47	1.62
Overshoot [°]	0	0.62	1.09
Steady state error [°]	0.08	1.29	2.03

To assess the controllability and stability of the system, a step response test was conducted. The system was driven to a target angle of 90° and the results of different load conditions are compared and presented in Fig. 7. As for the static load test, the maximum velocity and acceleration parameters are selected. In the case of the 2500 g load, the maximum rise time is 1.62 s with a maximal overshoot of 1.83% of the traveled range. The steady-state error stays for all load conditions below 2.03°. The step response showed that the elbow can be moved and held at a certain position over its full range of lifting capacity with a maximum rise time of 24 ms.

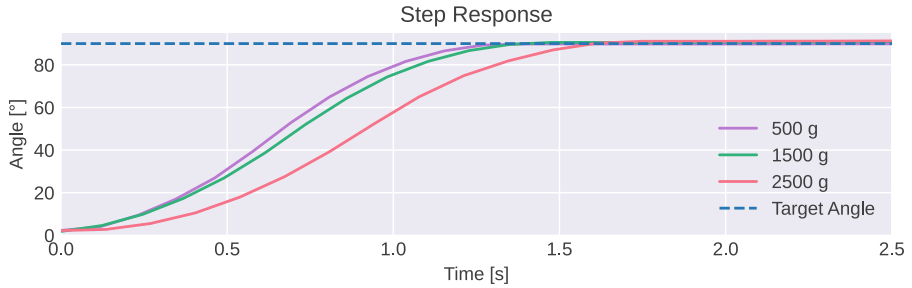

Fig. 7. Step response of BICEP in three different load conditions (500 g, 1500 g and 2500 g). The elbow was moved from 0° to 90° with maximum acceleration to its maximum speed.

3.5 Sideway Perturbation

An important feature of the compliant cross-axis flexural pivot joint used in BICEP is the possibility to absorb sideway perturbations through passive displacement. This allows to compensate for the lack of shoulder external rotation of conventional rigid sockets and partially absorb unexpected shocks. To estimate the displacement in this direction, the same experimental setup was used but with the system mounted sideways (perpendicular to the sagittal plane) to the table, so that the lower arm link is deformed

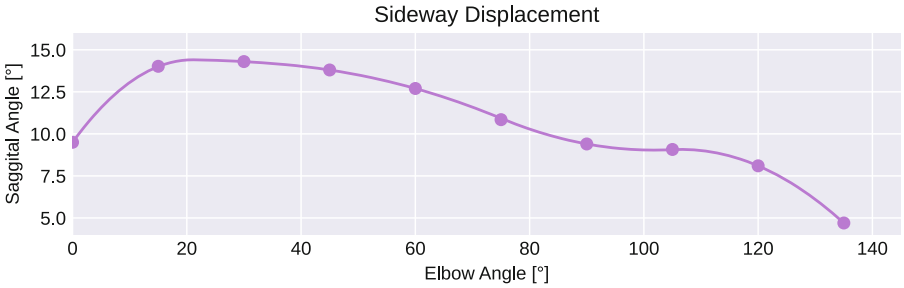

Fig. 8. Sideway displacement of BICEP for different angles ranging from 0° to 135° with 500 g load condition. For this experiment the BICEP was mounted sideway to the table. The plot shows a maximum displacement of 14.3°.

by gravity. The position of the elbow was increased in steps of 15° within a range from 0° to 135°. Only the adapter (weight of 500 g) was attached to the terminal part of the lower arm link to simulate the presence of an end-effector. The results of this validation, presented in Fig. 8, show a maximum displacement of 14.3°. This value is above our before-set requirement (>10°) and close to the human anatomical range (11.2°). The joint maintains this sagittal displacement below a flexion angle of 82°. Furthermore, we qualitatively performed a perturbation test at different commanded angles (θ): 135°, 90°, 45°, and 5°. In this case, we used the previous setup with the ground link of the elbow attached vertically. For each position, the elbow was set in the neutral configuration and an operator applies a lateral force at the terminal part of the lower arm link until the maximum transversal excursion is reached. The same validation was performed for both medial and lateral humeral rotation, as shown in Fig. 9. The range of motion was calculated using the software Tracker and presented in Fig. 9. A RoM of 20° is measured at $\theta = 20°$, and increases up to $\theta = 90°$, where the joint experiences its maximum compliance (RoM = 40°).

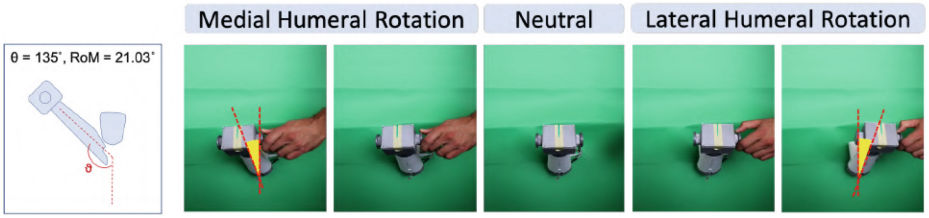

(a) Elbow position $\theta = 135°$

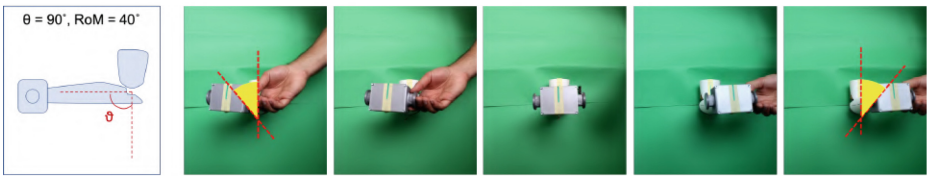

(b) Elbow position $\theta = 90°$

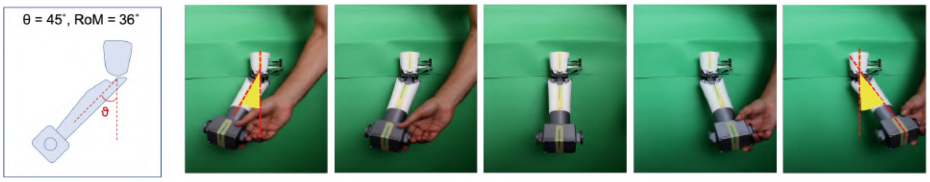

(c) Elbow position $\theta = 45°$

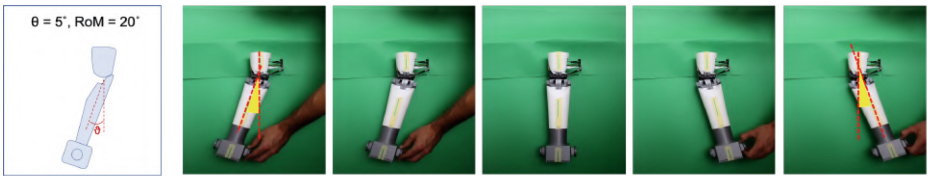

(d) Elbow position $\theta = 5°$

Fig. 9. Preliminary evaluation of the absorption of sideway perturbations. A schematic represents the elbow configuration from a lateral view, while the photo sequence shows a frontal view. For each position, an operator is applying a lateral force in each direction (medial and lateral humeral rotation), to reach the maximum range of motion (RoM). In each row, the central picture shows the neutral configuration, while the medial humeral rotation is presented in the left panels and the lateral humeral rotation in the right ones. The calculated RoM is presented next to each row.

4 Conclusion

We propose a novel prosthetic elbow (BICEP) using soft robotic technologies to improve its adaptability through the use of two cross-axis flexural pivots. A first prototype of BICEP was implemented and a preliminary characterization, including static and dynamic conditions, has been performed to evaluate the main features of this design. The outcome of the experimental validation demonstrates comparable results, in

terms of, weight (351 g), lifting capacity (up to 2500 g) and a maximum speed (157°/s), to state-of-art systems (reported in Tab. 1). Even though the positive results of the step response and the steady state error, the irregularities observed in the current consumption and deflection of the cross flexures show the need for a future extensive characterization with multiple repetitions. A set of preliminary qualitative experiments demonstrated an increase of the RoM on the transversal plane and the capability to absorb sideway perturbations in different configurations. These features could be interesting for both, amputees using conventional rigid sockets, or with osseointegration interfaces. Future work will focus on the optimization of the cross-axis flexural pivot design to achieve the desired stiffness and strength and to reduce the buckling effect. Current and deflection irregularities may be reduced by the use of a tendon tensioning mechanism. Finally, we will explore the advantages of the improved system in activities of daily living including subjects with limb loss.

Acknowledgments. This research project/publication was supported by TUM AGENDA 2030, funded by the Federal Ministry of Education and Research (BMBF) and the Free State of Bavaria under the Excellence Strategy of the Federal Government and the Länder as well as by the High-tech Agenda Bavaria.

The authors would like to thank Daniel Rixen and Simon Gerer for their valuable help with the manufacture of some components for the first prototype.

References

1. Farina, D., et al.: Toward higher-performance bionic limbs for wider clinical use. Nat. Biomed. Eng. **7**, 473–485 (2021)
2. De Groot, J.H., Angulo, S.M., Meskers, C.G., Van Der Heijden-Maessen, H.C., Arendzen, J.H.H.: Reduced elbow mobility affects the flexion or extension domain in activities of daily living. Clin. Biomech. **26**(7), 713–717 (2011)
3. Metzger, A.J., Dromerick, A.W., Holley, R.J., Lum, P.S.: Characterization of compensatory trunk movements during prosthetic upper limb reaching tasks. Arch. Phys. Med. Rehabil. **93**(11), 2029–2034 (2012)
4. Bandara, D., Gopura, R., Hemapala, K., Kiguchi, K.: Upper extremity prosthetics: current status, challenges and future directions. In: The Seventeenth International Symposium on Artificial Life and Robotics, vol. 2012 (2012)
5. Ottobock: DynamicArm Plus. https://www.ottobock.com/en-us/product/12K110N
6. Fillauer: Motion E2 Elbow. https://fillauer.com
7. Fillauer: Utah Arm 3+. https://fillauer.com/products/utah-arm-3-2
8. Steeper: Espire Pro. https://www.steepergroup.com
9. Ortiz-Catalan, M., Håkansson, B, Brånemark, R.: An osseointegrated human-machine gateway for long-term sensory feedback and motor control of artificial limbs. Sci. Transl. Med. **6**(257), 257re6–257re6 (2014)
10. Bennett, D.A., Mitchell, J., Goldfarb, M.: Design and characterization of a powered elbow prosthesis. In: Proceedings of the Annual International Conference of the IEEE Engineering in Medicine and Biology Society, EMBS, vol. 2015, November 2015
11. Chatterjee, A., Das, S., Verma, S.: Design of above elbow prosthesis articulated with electromyogram signal and electrical switch. J. Sci. Indus. Res. **78**, 8 (2019)
12. Piazza, C., Grioli, G., Catalano, M., Bicchi, A.: A century of robotic hands. Ann. Rev. Control Robot. Auton. Syst. **2**, 1–32 (2019)

13. Capsi-Morales, P., Grioli, G., Piazza, C., Bicchi, A., Catalano, M.G.: Exploring the role of palm concavity and adaptability in soft synergistic robotic hands. IEEE Robot. Autom. Lett. **5**(3), 4703–4710 (2020)
14. Deimel, R., Brock, O.: A novel type of compliant and underactuated robotic hand for dexterous grasping. Int. J. Robot. Res. **35**(1-3), 161–185 (2016). https://doi.org/10.1177/0278364915592961
15. Puhlmann, S., Harris, J., Brock, O.: RBO Hand 3: a platform for soft dexterous manipulation. IEEE Trans. Robot. **38**, 1–16 (2022)
16. Bilancia, P., Baggetta, M., Berselli, G., Bruzzone, L., Fanghella, P.: Design of a bio-inspired contact-aided compliant wrist. Robot. Comput. Integr. Manuf. **67**, 102028 (2021)
17. Montagnani, F., Smit, G., Controzzi, M., Cipriani, C., Plettenburg, D.H.: A passive wrist with switchable stiffness for a body-powered hydraulically actuated hand prosthesis. In: IEEE International Conference on Rehabilitation Robotics (2017)
18. Della Santina, C., Catalano, M.G., Bicchi, A., Ang, M., Khatib, O., Siciliano, B.: Soft robots. Encycl. Robot. **489**, 1–14 (2021)
19. Lenzi, T., Lipsey, J., Sensinger, J.W.: The RIC Arm - a small Anthropomorphic Transhumeral Prosthesis. IEEE/ASME Trans. Mechatron. **21**(6), 2660–2671 (2016)
20. Sensinger, J.W., et al.: User-modulated impedance control of a prosthetic elbow in unconstrained, perturbed motion. IEEE Trans. Biomed. Eng. **55**(3), 1043–1055 (2008)
21. Lemerle, S., Grioli, G., Bicchi, A., Catalano, M.G.: A variable stiffness elbow joint for upper limb prosthesis. In: IEEE International Conference on Intelligent Robots and Systems (2019)
22. Soucie, J., et al.: Range of motion measurements: reference values and a database for comparison studies. Haemophilia **17**(3), 500–507 (2011)
23. Jensen, B.D., Howell, L.L.: The modeling of cross-axis flexural pivots. Mech. Mach. Theory. **37**(2002), 461–476 (2002)
24. Podgórski, A., Kordasiewicz, B., Urban, M., Michalik, D., Pomianowski, S.: Biomechanical assessment of Varus-valgus range of motion of normal elbow joint using UB-01 measuring device. Ortopedia Traumatologia Rehabilitacja **14**(2), 137–144 (2012)
25. Buckley, M.A., Yardley, A., Johnson, G.R., Carus, D.A.: Dynamics of the upper limb during performance of the tasks of everyday living - a review of the current knowledge base. In: Proceedings of the Institution of Mechanical Engineers, Part H: Journal of Engineering in Medicine, vol. 210, no. 4 (1996)
26. Lee, Y.-T., Choi, H.-R., Chung, W.-K., Youm, Y.: Stiffness control of a coupled tendon-driven robot hand. IEEE Control Syst. Mag. **14**(5), 10–19 (1994)
27. Grebenstein, M., Chalon, M., Hirzinger, G., Siegwart, R.: Antagonistically driven finger design for the anthropomorphic DLR hand arm system. In: 2010 10th IEEE-RAS International Conference on Humanoid Robots, pp. 609–616 (2010)
28. Murray, I.A., Johnson, G.R.: A study of the external forces and moments at the shoulder and elbow while performing every day tasks. Clinical Biomech. **19**(6), 586–594 (2004)
29. Gates, D.H., Walters, L.S., Cowley, J., Wilken, J.M., Resnik, L.: Range of motion requirements for upper-limb activities of daily living. Am. J. Occup. Therapy. **70**, 70013500010 (2016)
30. Open Source Physics: Tracker. https://physlets.org/tracker/